Published in final edited form as:
J Mol Spectrosc. 2017 July ; 337: 90–95. doi:10.1016/j.jms.2017.04.001.

On the competition between weak O-H···F and C-H···F hydrogen bonds, in cooperation with C-H···O contacts, in the difluoromethane – *tert*-butyl alcohol cluster

Lorenzo Spada[a,*], **Nicola Tasinato**[a,*], **Giulio Bosi**[b], **Fanny Vazart**[a], **Vincenzo Barone**[a], and **Cristina Puzzarini**[b,*]

[a]Scuola Normale Superiore, Piazza dei Cavalieri 7, I-56126 Pisa (Italy)

[b]Dipartimento di Chimica ″G. Ciamician″ dell'Università di Bologna, Via Selmi 2, I-40126 Bologna, Italy

Abstract

The 1:1 complex of tert-butyl alcohol with difluoromethane has been characterized by means of a joint experimental-computational investigation. Its rotational spectrum has been recorded by using a pulsed-jet Fourier-Transform microwave spectrometer. The experimental work has been guided and supported by accurate quantum-chemical calculations. In particular, the computed potential energy landscape pointed out the formation of three stable isomers. However, the very low interconversion barriers explain why only one isomer, showing one O-H···F and two C-H···O weak hydrogen bonds, has been experimentally characterized. The effect of the H → *tert*-butyl- group substitution has been analyzed from the comparison to the difluoromethane-water adduct.

Keywords

Weak hydrogen bonds; rotational spectroscopy; quantum chemistry; DFT calculations; Non-covalent interactions

Introduction

Weak hydrogen bond (WHB) is, together with hydrogen (HB) [1] and halogen bond (HaB) [2], the most widespread non-covalent interaction encountered in nature, governing processes such as molecular association [3,4], microsolvation of organic molecules [5,6], molecular recognition [7] and many others. Their X-H···Y layered contacts (where X and Y are the hydrogen bond donor and acceptor, respectively) are characterized by similar directionality of the HB, showing, however, blue shifts of the stretching frequencies of the X-H groups and dissociation energies of only a few kJ·mol^{-1}. Among WHBs, the interactions involving organic fluorine as hydrogen bond acceptor are of great interest because of the role they play, for example, in pharmaceutical [8], in functional materials [9] and in polymerization [10] fields.

*Corresponding authors: lorenzo.spada@sns.it; nicola.tasinato@sns.it; cristina.puzzarini@unibo.it.

Europe PMC Funders Author Manuscripts

Even if the weakness of organic fluorine as hydrogen bond acceptor (HBa) is well established [11–13], the formation of C-H···F-C or O-H···F-C WHBs is the mechanism at the basis of the crystal packing of fluoroaromatic compounds [13] or the stabilization in solid, alkane solution [14], and in the gas phase of some fluoroalcohol compounds [15–16], respectively, for the latter in association with O-H···O HBs. In this respect, when it is possible a competition between these two WHBs involving organic fluorine as HBa, which of the aforementioned non-covalent interactions is favorite? Aiming at answering to this question, in the present study, we report a combined quantum-chemical and rotational study of the difluoromethane (DFM) – tert-butyl alcohol (TBA) cluster where the competition between C-H···F-C and O-H···F-C WHBs, in combination with C-H···O contacts, is possible. Our goal is to combine the capability of rotational spectroscopy in supersonic expansion with high-level quantum-chemical calculations to explore the potential energy surface of the dimer and to unveil the genuine nature of these WHBs in an environment free from solvent and matrix effects. Furthermore, thanks to a previous microwave characterization of the O-H···F-C WHB, together with two C-H···O interactions, in the DFM-water complex [17–19], the influence of substituent (*tert*-butyl of TBA vs hydrogen of water) on the cluster bonding energy can be also directly evaluated.

The manuscript is organized as follows. In the next two sections the experimental and computational details are described. Subsequently, discussion and concluding remarks are provided.

Computational details

Our work began with exploratory quantum-chemical calculations of the relevant stationary points on the potential energy surface (PES) of the DFM-TBA complex employing density functional theory (DFT). To this purpose, the B3LYP functional [20,21] augmented by dispersion corrections according to Grimme's DFT-D3 scheme [22] in conjunction with the polarized double-ζ SNSD basis set [23,24] was used. We note that the D3 correction, which has been tested over a wide range of molecular systems (e.g. [25–31] and references therein), is fundamental for describing the thermochemistry of van der Waals adducts with DFT, because most of the density functionals fail to correctly describe long-range dispersion correlation effects.

Geometry optimizations were carried out first, and then at the optimized structure harmonic frequencies were computed through analytical hessians [32]. In addition, for each identified stationary point, in order to compute anharmonic contributions to vibrational frequencies, but also vibrational corrections to rotational constants (of interest for the minima structures), cubic and quartic semi-diagonal force constants were calculated in a normal mode representation by numerical differentiation of analytic quadratic force constants (a step size of 0.01 Å was used for displacements).

In a subsequent step, for all stationary points, optimized structures and harmonic force fields were further refined by using the double-hybrid B2PLYP-D3 functional [33] coupled to the m-aug-cc-pVTZ basis set [34], in which *d*-functions on H atoms were removed. In the following, this basis set is referred to as m-aug-cc-pVTZ-*d*H. Figure 1 provides a graphical

overview of the stationary points located on the PES and of their interconnection. To evaluate improved zero-point vibrational energies (ZPE) beyond the harmonic approximation, B2PLYP-D3/m-aug-cc-pVTZ-*d*H harmonic frequencies were then coupled with B3LYP-D3/SNSD cubic and semi-diagonal quartic force constants to formulate a hybrid B2PLYP/B3LYP anharmonic force field. To determine ZPE, the hybrid degeneracy corrected perturbation theory to second order (HDCPT2) was employed [35,36].

The equilibrium structures at the B2PLYP-D3/m-aug-cc-pVTZ-*d*H level were used as starting point for computing vibrational ground-state rotational constants and accurate electronic energies. In fact, equilibrium structures straightforwardly provide equilibrium rotational constants, B_e^α, which were corrected by adding the vibrational contributions, ΔB_0^α, thus obtaining the ground-state rotational constants, B_0^α :

$$B_0^\alpha = B_e^\alpha + \Delta B_0^\alpha \quad (1)$$

where α denotes the principal inertia axis (α = *a, b, c*; thus $B_0^\alpha = A_0, B_0, C_0$). Vibrational corrections were obtained by means of second-order vibrational perturbation theory (VPT2) [37–39] applied to the molecular ro-vibrational Watson Hamiltonian expressed in normal coordinates (e.g. see Ref. [40] and references therein).

Accurate electronic energies were obtained as single-point computations at the B2PLYP-D3/m-aug-cc-pVTZ-*d*H optimized structures by means of the composite scheme described here below. In this scheme, the different contributions are evaluated at the highest level possible, yet maintaining the overall computational cost affordable in terms of both hardware requirements and computational costs. This computational protocol takes the coupled-cluster theory employing the singles and doubles approximation augmented by a perturbative treatment of triple excitations, CCSD(T) [41,42], as starting point. The energy at the CCSD(T)/cc-pVTZ [43] level is then corrected for basis-set truncation error and core-correlation effects. The latter two contributions are evaluated at second-order Møller-Plesset perturbation theory (MP2) [44]. The best estimate of the electronic energy is then given by the equation [45,46]:

$$E_{\text{best}} = E(\text{CCSD(T)/VTZ}) + \Delta E(\text{MP2/CBS}) + \Delta E(\text{MP2/CV}) \quad (2)$$

The Δ*E*(MP2/CBS) is obtained by extrapolating the Hartree-Fock (HF-SCF) electronic energy, E_∞^{HF-SCF}, to the complete basis set (CBS) limit according to the e^{-Cn} functional form [47] using the cc-pV*n*Z with *n* = T, Q, 5 basis sets [43,48,49], and the MP2 correlation contribution by means of the n^{-3} formula [50] employing the cc-pVTZ and cc-pVQZ basis sets. Δ*E*(MP2/CV) represents the core-valence correlation correction, and is obtained as difference of MP2/cc-pCVTZ [51] energies evaluated correlating all electrons (a.e.) and within the frozen-core (f.c.) approximation:

$$\Delta E(\text{CV}) = E[(\text{MP2}/p\text{CVnZ(a.e.)}] - E[\text{MP2/pCVnZ(f.c.)}] \quad (3)$$

The same protocol was also applied to obtain best-estimated electronic energies of the isolated fragments, i.e., DFM and TBA, in order to evaluate best-estimated dissociation energies as the difference between the electronic energy of the DFM-TBA complex and those of the isolated monomers. The basis set superposition error (BSSE) was taken into account by means of the counterpoise correction (CP) procedure, introduced by Boys and Bernardi [52].

Finally, for the most stable isomer, the cubic and semi-diagonal quartic force field was also evaluated at the B2PLYP-D3/m-aug-cc-pVTZ-*d*H level in order to derive the partial effective structure r_0.

All DFT, HF-SCF and MP2 calculations were carried out by using a development version of the Gaussian software [53], while CCSD(T) computations were performed with the CFOUR program package [54].

Experimental methods and Rotational spectrum

The rotational spectrum of the 1:1 DFM:TBA cluster has been recorded using a COBRA-type [55] pulsed-jet Fourier-transform microwave (FTMW) spectrometer [56], described elsewhere [57], operating in the 6.5 – 18.5 GHz range. A gas mixture at 1% of CH_2F_2 (DFM) in Helium at a stagnation pressure of 0.2 MPa has been passed over a sample of tert-butyl alcohol (TBA), used without further purification, and expanded into the Fabry-Perot cavity, through the pulsed valve (General valve, series 9, nozzle diameter 0.5 mm). According to the quantum-chemical calculations, we started with the search of the rotational transitions belonging to the isomer M1, which is predicted to be the most stable one (see Figure 1), having a large value of the dipole moment component μ_a (2.6 D). Three rotational transitions around 7218.9, 7270.3 and 7325.8 MHz have been first observed and assigned to the $J = 6 \leftarrow 5$ band, with $K_a = 0, 1$, of the M1 isomer. Later on, other 93 μ_a-*R*-type lines up to $J_{upper} = 15$ and $K_a = 6$ (Figure 2, which depicts the $J = 7_{07} \leftarrow 6_{06}$ rotational transition, provides an example) and other 9 much weaker μ_b-*R*-type transitions have been identified and fitted using Pickett's SPFIT program [58] within Watson's semirigid Hamiltonian (*S*-reduction; I^r-representation) [59]. The results of the fit are reported in Table 1, while the complete list of transition frequencies is collected in the Supplementary Information (Table S1). No μ_c-type lines have been observed in agreement with the C_s symmetry of the cluster. The search for rotational transitions belonging to the M2 and M3 isomers failed due to plausible relaxation processes toward M1, taking place when the interconversion barrier values are lower than $2kT$ at room temperature [60], as suggested by the data reported on Figure 1.

As shown in Figure 2, transitions are split in doublets due to Doppler effect. The rest frequencies have been obtained as the arithmetic mean of the two component frequencies. The estimated accuracy of frequency measurements is better than 3 kHz, and the resolution is better than 7 kHz.

Europe PMC Funders Author Manuscripts

Discussion

Table 1 collects the experimental rotational parameters of the M1 isomer as obtained in the fitting procedure described above. This table also reports the corresponding computed values together with those of the M2 and M3 isomers. We note that the experimental rotational constants as well as the D_J and D_{JK} quartic centrifugal-distortion terms have been determined to a very good precision, while the other centrifugal-distortion constants are affected by larger uncertainties, ranging from 3% to 25%. We furthermore note a good agreement between the computed values and the experimental counterparts: A is predicted well within 1%, while deviations of about 2% are observed for B and C. According to the results of Table 1 as well as based on the relative energies collected in Figure 1 (the complete dataset is reported in the Supplementary Information: Table S2), there is no doubt concerning which isomer has been experimentally observed. Indeed, the isomerization path graphically summarized in Figure 1 explains the experimental outcome: at the equilibrium, both the M3-M2 and M2-M1 interconversion barriers are predicted to be only 0.03 kcal/mol at the best-estimated (composite scheme, see computational details) level. Even if the M2 isomer is predicted to be less stable than M1 by only 0.06 kcal/mol, the small interconversion barrier suggests that it easily relaxes to M1, thus preventing its observation. Even more significant are the conclusions that can be drawn once the equilibrium relative energies are corrected for ZPE (hybrid force field, see computational details). Indeed, ZPE-corrected energies (see Figure 1) suggest that the vibrational ground state of the M2 isomer is above the TS1 barrier, while that of M3 is as high in energy as TS2. The overall picture thus suggests that both M2 and M3 relax to M1, as experiment tends to support. According to the molecular structures depicted in Figure 1, the energies of the M1, M2 and M3 isomers are related to the number and type of WHBs involved in the cluster. In the case of M3, two C-H···F and one C-H···O interactions are established. The stabilization in energy moving to the M2 isomer can be explained in terms of the replacement of one C-H···F WHB with one O-H···F interaction. A further stabilization is then obtained once also the remaining C-H···F WHB is replaced by an additional O-H···F bond. We can thus conclude that the most stable structure (M1) is obtained when the largest number of C-H···O contacts are established together with the O-H···F WHB.

While the optimized geometries of the M1, M2 and M3 isomers at the B2PLYP/m-aug-cc-pVTZ-*d*H level are reported in the Supplementary Information (Table S3), in the context of this study more interesting is the partial effective structure (r_0) of M1 that can be derived from our data. This has been obtained by fitting two geometrical parameters (the distance $r_{O6\cdots C1}$ and angle O6···C1-F3 of Figure 3) while keeping the other ones fixed at their vibrationally averaged B2PLYP-D3/m-aug-cc-pVTZ-*d*H values (the calculated geometry is available as Supplementary Information, Table S4). In this way, the experimental rotational constants are perfectly reproduced, with the largest discrepancy, that on the A rotational constant, being well within 0.1%. The resulting values are reported in Table 2, where they are compared with the ones relative to the equilibrium structure (r_e). The conclusion that can be drawn is that the data of Table 2 further confirms that the level of theory chosen is able to well describe the structure of the molecular complex.

The results obtained in the present study allow us to discuss the hydrogen bond parameters in comparison with those of the DFM-water complex. The relevant parameters are collected in Table 3, with the corresponding atoms labeling shown in Figure 4 (with R= H- or *tert*-butyl-). According to the partial r_0 structure of Table 3, it is noted that when going from water to TBA as counterpart molecule in the cluster with DFM, the O-H···F distance increases of about 0.2 Å (2.20 Å vs. 2.384 Å). This is only in apparent contradiction with the stronger binding energy of the DFM-TBA complex (see later on in the manuscript). In fact, it is seen that at the B2PLYP/m-aug-cc-pVTZ-*d*H level the O-H···F distance increases by a smaller extent (2.306 Å vs 2.360 Å). Furthermore, for the C-H···O interaction, a shrinkage of the corresponding length is predicted when going from DFM-water to DFM-TBA (2.834 Å vs 2.784 Å). Furthermore, in the case of the water complexation of DFM, the internal rotation of water around its C_2 axis generates a tilted angle of 23° between the water plane and the ∠FCF angle of DFM, instead C_s symmetry is observed for the DFM-TBA adduct. The effect of the aforementioned motion affects, in particular, the O-H1···F1 angle value, while only a slightly difference is noted for the C1-F1···H1 angle (see Table 3) of both the DFM-water and DFM-TBA complexes.

The last information that can be obtained from our study is the dissociation energy of the complex. Based on the isomer structure depicted in Figure 3, the so-called “pseudo-diatomic approximation” can be assumed to estimate the force constant (k_s) of the intermolecular stretching between the centers of mass of DFM and TBA, because its axis is almost parallel to the *a*-axis of the cluster (as evident in Figure 3). According to this approximation, k_s can be written as [61]:

$$k_s = \frac{16\pi^4(\mu R_{\mathrm{CM}})^2 \left\lfloor 4B^4 + 4C^4 - (B-C)^2(B+C)^2 \right\rfloor}{hD_J} \quad (4)$$

where μ is the pseudo-diatomic reduced mass, R_{CM} the distance between the centers of mass of the two monomers (4.73 Å), and B, C and D_J the experimental values reported in Table 1. The k_s value obtained by applying Eq. (4) is 9.0 N·m^{-1}. Assuming a Lennard-Jones type potential, the dissociation energy is calculated according to the equation [62]:

$$E_D = \frac{1}{72} k_s (R_{\mathrm{CM}})^2 \quad (5)$$

thus obtaining a value of 4.02 kcal·mol^{-1}. This value is in good agreement with the best-estimated ZPE-corrected value, 3.56 kcal·mol^{-1} (reported in Table S2 of the Supplementary information), which is expected to have an accuracy of ~0.5 kcal·mol^{-1} [45,46]. Such an agreement suggests that, despite its limitations, the “pseudo-diatomic approximation” is able to provide a reliable determination of the dissociation energy. It is noted that this value is much larger than that estimated for DFM-water (1.79 kcal·mol^{-1}) [18]. This suggests that the size of the residual groups (R in Figure 4) of the R-O-H hydrogen bond donor sensibly affects the stability of the clusters linked by one O-H···F and 2 C-H···O WHBs. This suggestion has been further supported by computations at the B2PLYP-D3/m-aug-cc-pVTZ-

*d*H level. At this level of theory, the dissociation energy corrected by the ZPE contribution (evaluated using the B2PLYP/B3LYP hybrid force field) is 2.17 kcal/mol, to be compared with the value of 3.19 kcal/mol obtained for DFM-TBA at the same level of theory.

Conclusions

In the present study, the 1:1 complex of *tert*-butyl alcohol with difluoromethane has been accurately characterized by means of experimental and computational techniques. Starting from an accurate sampling of the potential energy surface, the structure and energetics of the complex have been obtained from the investigation of its rotational spectrum, which has been guided and complemented by accurate quantum-chemical calculations.

The C_s symmetric M1 isomer, whose stability is due to the formation of one O-H···F and two C-H···O WHBs, has been experimentally confirmed to be the global minimum. The failure in the observation of the rotational spectra of the M2 and M3 isomers, whose monomers are linked by one O-H···F, one C-H···F, one C-H···O and two C-H···F, one C-H···O WHBs, respectively, has been plausibly ascribed to the relaxation processes toward the M1 isomer taking place in the supersonic expansion. The H → *tert*-butyl substitution effect, observed when going from DFM-water to DFM-TBA 1:1 cluster, has been evaluated, resulting in an increase of the bonding energy of the adduct. The weakness of the hydrogen bonds established in the complex is further confirmed by the energy dissociation, which has been accurately computed to be 3.6 kcal·mol^{-1}, value also confirmed by an analysis based on the so-called “pseudo-diatomic approximation”.

Supplementary Material

Refer to Web version on PubMed Central for supplementary material.

Acknowledgements

This work was supported by Italian MIUR (PRIN 2012 “STAR: Spectroscopic and computational Techniques for Astrophysical and atmospheric Research”), by the University of Bologna (RFO funds), and by Scuola Normale Superiore (funds for project “COSMO: Combined experimental and computational spectroscopic modeling for astrochemical applications”). The support of the COST CMTS-Action CM1405 (MOLIM: MOLecules In Motion) is also acknowledged. The research leading to these results has received funding from the European Union’s Seventh Framework Programme (FP/ 2007-2013) under the grant agreement no. ERC-2012-AdG-320951-DREAMS. The SMART@SNS Laboratory (http://dreams.sns.it) is acknowledged for providing high performance computer facilities.

References

[1]. Arunan E, Desiraju GR, Klein RA, Sadlej J, Scheiner S, Alkorta I, Clary DC, Crabtree RH, Dannenberg JJ, Hobza P, Kjaergaard HG, et al. Pure Appl Chem. 2011; 83:1637–1641. ©IUPAC.

[2]. Desiraju GR, Ho PS, Kloo L, Legon AC, Marquardt R, Metrangolo P, Politzer P, Resnati G, Rissanen K. Pure Appl Chem. 2013; 85:1711–1713. ©IUPAC.

[3]. Feng G, Evangelisti L, Cacelli I, Carbonaro L, Prampolini G, Caminati W. Chem Commun. 2014; 50:171–173.

[4]. Tatamitani Y, Liu BX, Shimada J, Ogata T, Ottaviani P, Maris A, Caminati W, Alonso JL. J Am Chem Soc. 2002; 124:2739–2743. [PubMed: 11890825]

[5]. Perez C, Neill JL, Muckle MT, Zaleski DP, Pena I, Lopez JC, Alonso JL, Pate BH. Angew Chem Int Ed. 2015; 54:979–982.

[6]. Gou Q, Spada L, Lòpez JC, Grabow J-U, Caminati W. Chem Asian J. 2015; 10:1198–1203. [PubMed: 25677836]
[7]. Bissantz C, Kuhn B, Stahl M. J Med Chem. 2010; 53:5061–5084. [PubMed: 20345171]
[8]. Müller K, Faeh C, Diederich F. Science. 2007; 317:1881–1886. [PubMed: 17901324]
[9]. Berger R, Resnati G, Metrangolo P, Weberd E, Hulliger J. Chem Soc Rev. 2011; 40:3496–3508. [PubMed: 21448484]
[10]. Kui SCF, Zhu N, Chan MCW. Kui SCF, Zhu N, Chan MCW. Angew Chem. Angew Chem Int Ed. 2003; 2003; 11542:1666–1670. 1628–1632.
[11]. Howard JAK, Hoy VJ, O'Hagan D, Smith GT. Tetrahedron. 1996; 52:12613–12622.
[12]. Dunitz JD, Taylor R. Chem Eur J. 1997; 3:89–98.
[13]. Thalladi VR, Weiss H-C, Bläser D, Boese R, Nangia A, Desiraju GR. J Am Chem Soc. 1998; 120:8702–8710.
[14]. Barbarich TJ, Rithner CD, Miller SM, Anderson OP, Strauss SH. J Am Chem Soc. 1999; 121:4280–4281.
[15]. Liu X, Borho N, Xu Y. Chem Eur J. 2009; 15:270–277. [PubMed: 19040230]
[16]. Thomas J, Liu X, Jäger W, Xu Y. Angew Chem Int Ed. 2015; 54:11711–11715.
[17]. Caminati W, Melandri S, Schnell M, Banser D, Grabow J-U, Alonso JL. Journal of Molecular Structure. 2005; 742:87–90.
[18]. Caminati W, Melandri S, Rossi I, Favero PG. J Am Chem Soc. 1999; 121:10098–10101.
[19]. Evangelisti L, Feng G, Gou Q, Guidetti G, Caminati W. Spectrochim Acta A. 2015; 136:64–67.
[20]. Lee C, Yang W, Parr RG. Phys Rev B. 1988; 37:785–789.
[21]. Becke AD. J Chem Phys. 1993; 98:5648–5652.
[22]. Grimme S, Anthony J, Ehrlich S, Krieg H. J Chem Phys. 2010; 132:154104/1–154104/19. [PubMed: 20423165]
[23]. Carnimeo I, Puzzarini C, Tasinato N, Stoppa P, Pietropolli Charmet A, Biczysko M, Cappelli C, Barone V. J Chem Phys. 2013; 139:074310/1–16. [PubMed: 23968095]
[24]. http://dreamslab.sns.it/
[25]. Goerigk L, Grimme S. Phys Chem Chem Phys. 2011; 13:6670–6688. [PubMed: 21384027]
[26]. Grimme S. Chem Eur J. 2012; 18:9955–9964. [PubMed: 22782805]
[27]. Delle Piane M, Corno M, Ugliengo P. J Chem Theo Comput. 2013; 9:2404–2415.
[28]. Delle Piane M, Vaccari S, Corno M, Ugliengo P. J Phys Chem A. 2014; 118:5801–5807. [PubMed: 24467179]
[29]. Tasinato N, Grimme S. Phys Chem Chem Phys. 2015; 17:5659–5669. [PubMed: 25623466]
[30]. Sure R, Grimme S. J Chem Theo Comput. 2015; 11:3785–3801.
[31]. Tasinato N, Moro D, Stoppa S, Pietropolli Charmet A, Toninello P, Giorgianni S. Appl Surf Sci. 2015; 353:986–994.
[32]. Biczysko M, Panek P, Scalmani G, Bloino J, Barone V. J Chem Theo Comput. 2010; 6:2115–2125.
[33]. Grimme S. J Chem Phys. 2006; 124:034108/1–16. [PubMed: 16438568]
[34]. Papajak E, Leverentz HR, Zheng J, Truhlar DG. J Chem Theo Comput. 2009; 5:1197–1202.
[35]. Bloino J, Biczysko M, Barone V. J Chem Theo Comput. 2012; 8:1015–1036.
[36]. Pietropolli Charmet A, Stoppa P, Tasinato N, Giorgianni S, Barone V, Biczysko M, Bloino J, Cappelli C, Carnimeo I, Puzzarini C. J Chem Phys. 2013; 139:164302/1–15. [PubMed: 24182024]
[37]. Papoušek, D., Aliev, MR. Molecular Vibrational/Rotational Spetra. Elesevier; Amsterdam: 1982.
[38]. Mills, IM. Molecular Spectroscopy: Modern Research. Rao, K. Narahari, Mathews, C. Weldon, editors. Academic Press; p. 115-140.
[39]. Amos RD, Handy NC, Green WH, Jayatilaka D, Willets A, Palmieri P. J Chem Phys. 1991; 95:8323–8336.
[40]. Penocchio E, Mendolicchio M, Tasinato N, Barone V. Can J Chem. 2016; 94:1065–1076.
[41]. Purvis GD III, Bartlett RJ. J Chem Phys. 1982; 76:1910–1918.

[42]. Raghavachari K, Trucks GW, Pople JA, Head-Gordon M. Chem Phys Lett. 1989; 157:479–483.
[43]. Kendall RA, Dunning TH Jr, Harrison RJ. J Chem Phys. 1992; 96:6796–6806.
[44]. Møller C, Plesset MS. Phys Rev. 1934; 46:618–622.
[45]. Puzzarini C, Biczysko M, Barone V, Largo L, Peña I, Cabezas C, Alonso JL. J Phys Chem Lett. 2014; 5:534–540. [PubMed: 26276605]
[46]. Puzzarini C, Biczysko M. J Phys Chem A. 2015; 119:5386–5395. [PubMed: 25474644]
[47]. Feller D. J Chem Phys. 1993; 98:7059–7071.
[48]. Woon DE, Dunning TH Jr. J Chem Phys. 1993; 98:1358–1371.
[49]. Peterson KA, Woon DE, Dunning TH Jr. J Chem Phys. 1994; 100:7410–7415.
[50]. Helgaker T, Klopper W, Koch H, Noga J. J Chem Phys. 1997; 106:9639–9646.
[51]. Peterson KA, Dunning TH Jr. J Chem Phys. 2002; 117:10548–10560.
[52]. Boys SF, Bernardi F. Mol Phys. 1970; 19:553–566.
[53]. Frisch, MJ., Trucks, GW., Schlegel, HB., Scuseria, GE., Robb, MA., Cheeseman, JR., Scalmani, G., Barone, V., Mennucci, B., Petersson, GA., Nakatsuji, H., et al. Gaussian Development Version, revision I.04+. Gaussian, Inc; Wallingford CT: 2009.
[54]. Stanton JF, Gauss J, Harding ME, Szalay PG, Auer AA, Bartlett RJ, Benedikt U, Berger C, Bernholdt DE, Bomble YJ, Cheng L, et al. CFOUR, a quantum chemical program package.
[55]. Grabow J-U, Stahl W, Dreizler H. Rev Sci Instrum. 1996; 67:4072–4084.
[56]. Balle TJ, Flygare WH. Rev Sci Instrum. 1981; 52:33–45.
[57]. Caminati W, Millemaggi A, Alonso JL, Lesarri A, Lopez JC, Mata S. Chem Phys Lett. 2004; 392:1–6.
[58]. Pickett HM. J Mol Spectrosc. 1991; 148:371–377.
[59]. Watson, JKG. Vibrational Spectra and Structure. Durig, JR., editor. Vol. 6. Elsevier; New York/ Amsterdam: 1977. p. 1-89.
[60]. Ruoff RS, Klots TD, Emilsson T, Gutowsky HS. J Chem Phys. 1990; 93:3142–3150.
[61]. Millen DJ. Can J Chem. 1985; 63:1477–1479.
[62]. Novick SE, Harris SJ, Janda KC, Klemperer W. Can J Phys. 1975; 53:2007–2015.

Europe PMC Funders Author Manuscripts

Europe PMC Funders Author Manuscripts

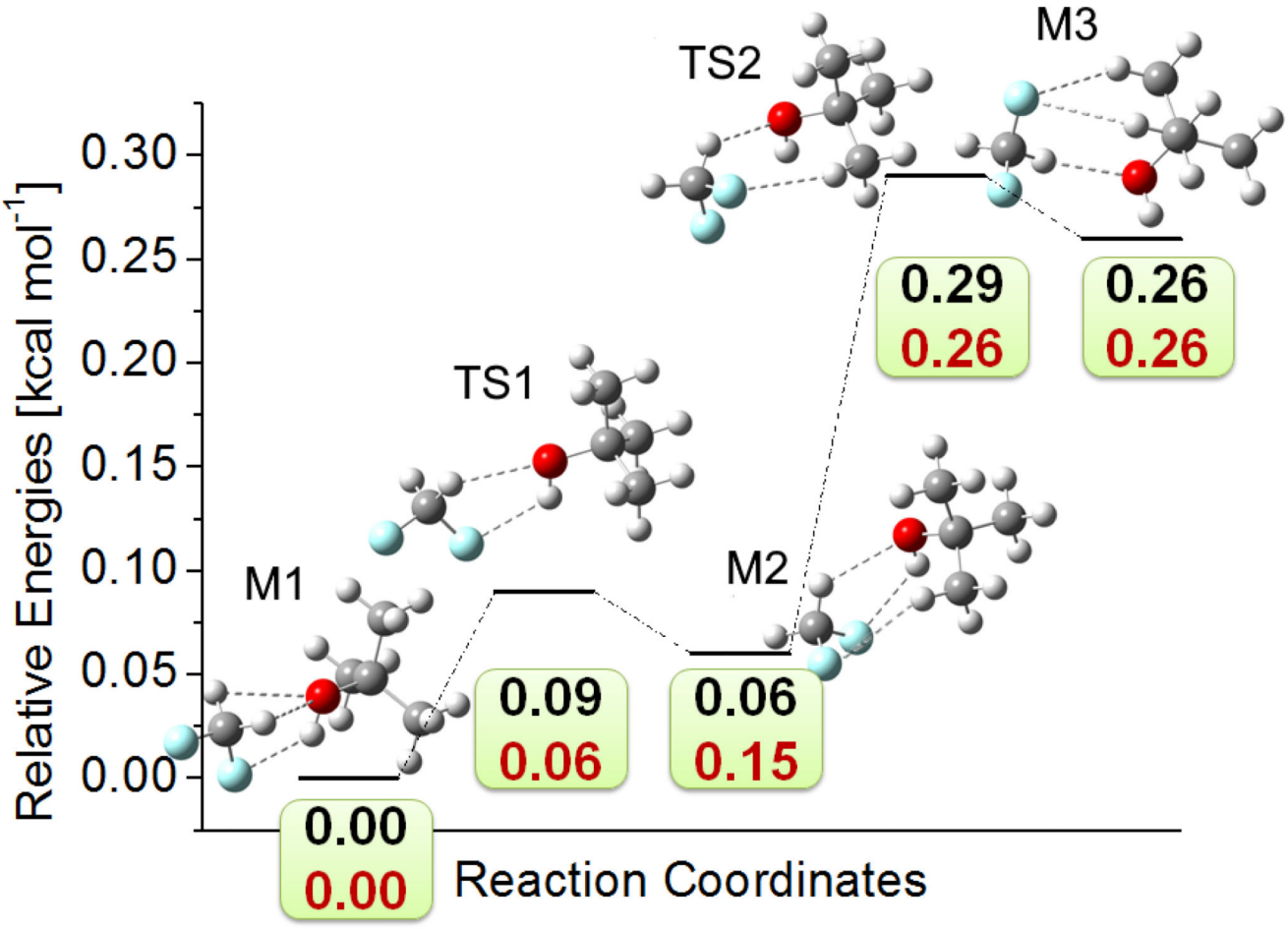

Figure 1.

Potential energy surface of the DFM – TBA cluster showing the structures of the three minima (M1, M2, M3) and the two transition states (TS1, TS2). The best-estimated relative electronic energies (black values) and the best-estimated relative electronic energies corrected by anharmonic ZPE computed from hybrid B2PLYP-D3/m-aug-cc-pVTZ-dH/B3LYP-D3/SNSD force field (red values) are also reported.

Europe PMC Funders Author Manuscripts

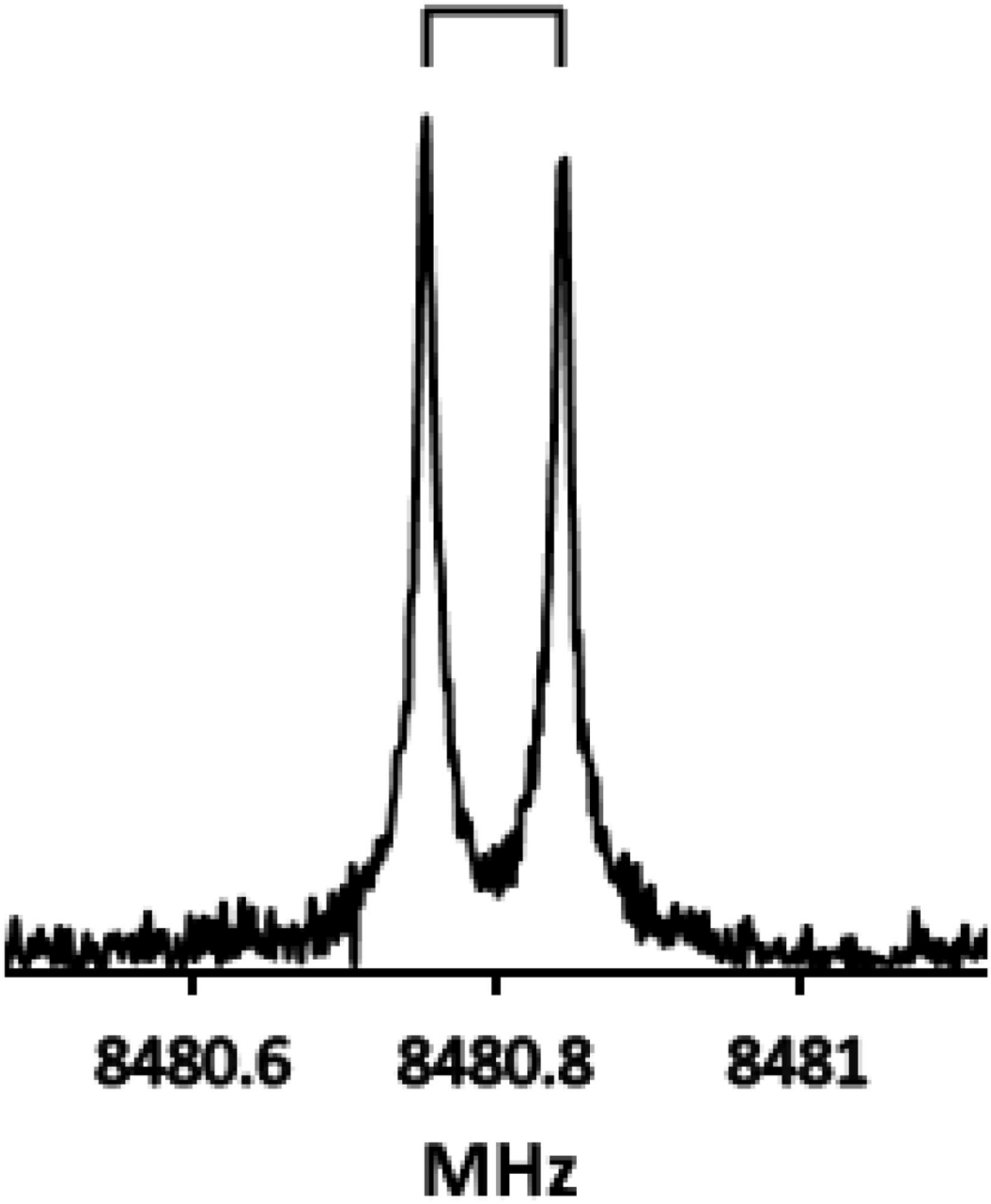

Figure 2.
The $J = 7_{07} \leftarrow 6_{06}$ rotational transition of the M1 isomer of the DFM-TBA cluster.

Europe PMC Funders Author Manuscripts

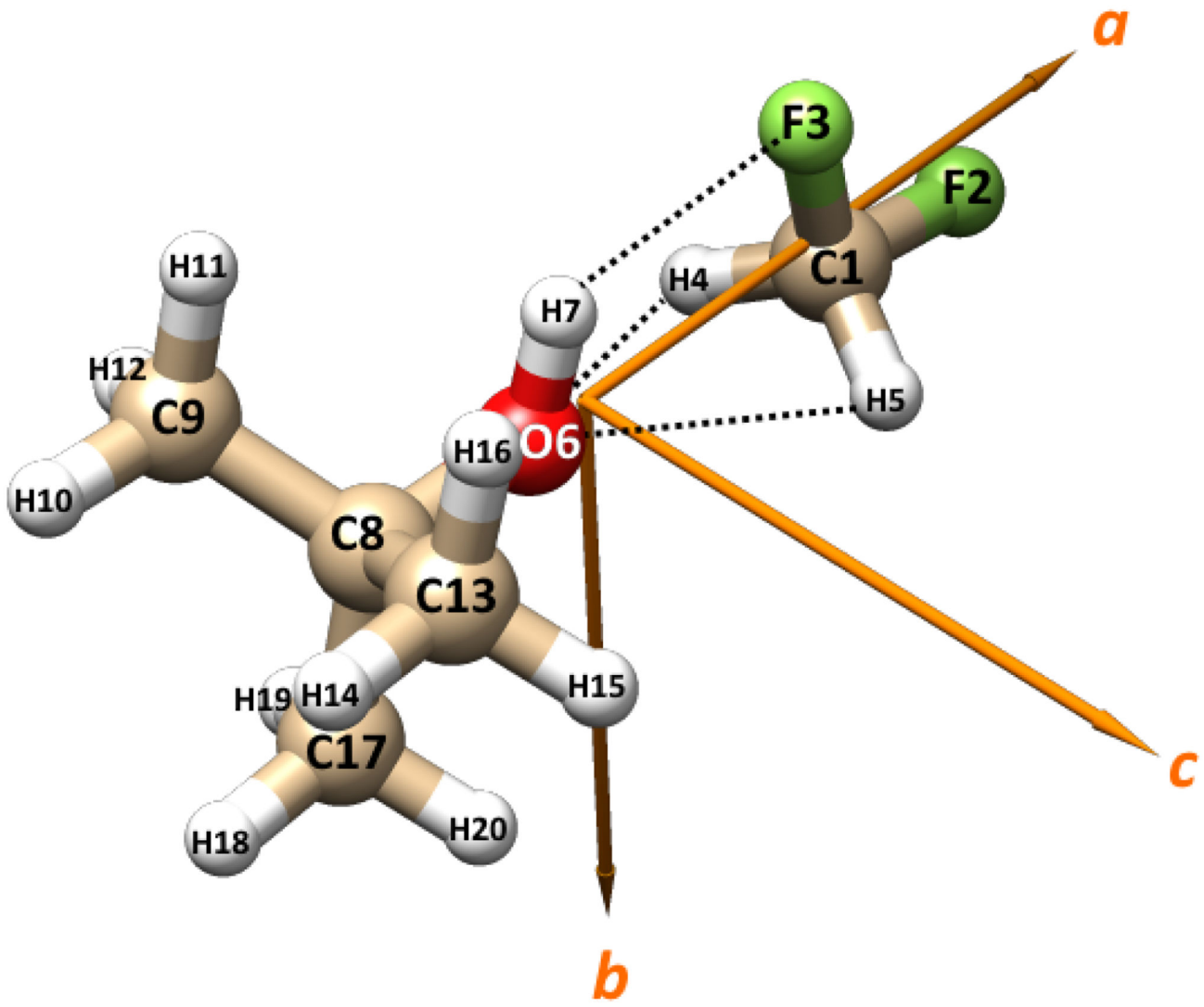

Figure 3.
The structure (with atom numbering) of the M1 isomer of DFM-TBA orientated with respect to the principal axes of inertia (*a*,*b*,*c*).

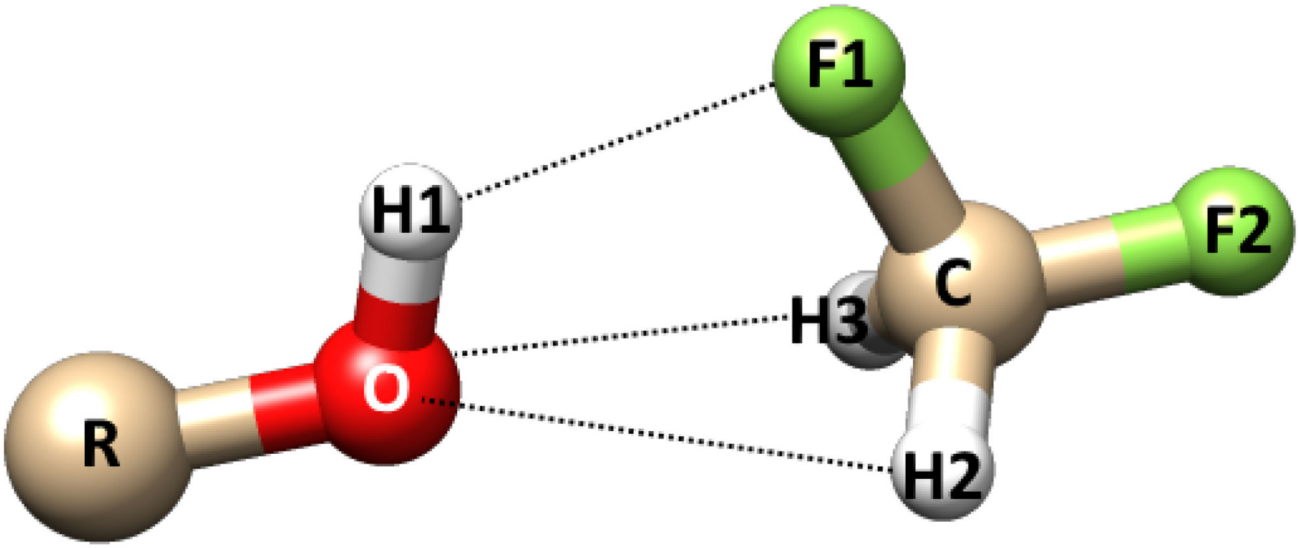

Figure 4.
Schematic representation of the DFM−R-OH hydrogen bonded complex. The atom labeling is also reported.

Europe PMC Funders Author Manuscripts

Table 1

Rotational parameters and dipole moment components for the M1, M2 and M3 isomers of DFM-TBA.

	M1		M2	M3
	Experiment[a]	**Theory**[b]	**Theory**[b]	**Theory**[b]
A / MHz	3602.299(3)	3570	3137	3064
B / MHz	615.0150(1)	601	780	772
C / MHz	597.1948(1)	584	742	732
D_J / kHz	0.1630(1)	0.15	1.33	0.98
D_{JK} / kHz	7.672(2)	7.63	7.45	6.29
D_K / kHz	-2.8(7)	-3.86	-6.90	-4.28
d_1 / Hz	-5.2(2)	-5.78	-104.37	-76.24
d_2 / Hz	4.3(1)	4.47	3.73	3.46
σ [c]/kHz	2.8			
N [d]	105			
$\lvert\mu_a\rvert$ [e] / D		2.55	1.49	0.34
$\lvert\mu_b\rvert$ [e] / D		0.63	0.49	0.04
$\lvert\mu_c\rvert$ [e] / D		0.00	0.78	0.42

[a] Standard error in parentheses in units of the last digit.

[b] B2PLYP-D3/aug-cc-pVTZ-*d*H equilibrium parameters. Equilibrium rotational constants have been augmented by vibrational corrections at the B3LYP-D3/SNSD level (see text).

[c] Standard deviation of the fit.

[d] Number of fitted transitions.

[e] Absolute values of the dipole moment components: B2PLYP-D3/aug-cc-pVTZ-*d*H equilibrium values augmented by vibrational corrections at the B3LYP-D3/SNSD level.

Europe PMC Funders Author Manuscripts

Table 2

Comparison between the fitted effective structure and the B2PLYP-D3/m-aug-cc-pVTZ-*d*H calculated values of the observed (M1) DFM-TBA cluster.

	r_0		r_e
	Exp	*Theory*	
$r_{O6\cdots C1}$ / Å	2.960(2)	2.993	2.966
∠O6···C1-F3 / °	73.7(1)	74.6	74.2

Europe PMC Funders Author Manuscripts

Table 3

Comparison of the parameters involved in the WHBs of the DFM-TBA and DFM-water complexes.

Weak hydrogen bond parameters				
	DFM-TBA		DFM-water	
	r_0	r_e	r_0 [a]	r_e
$r_{H1\cdots F1}$ / Å	2.384	2.360	2.20(1)	2.306
$r_{H2\cdots O} = r_{H3\cdots O}$ / Å	2.781	2.784	-	2.834
∠O-H1···F1 / °	113.1	115.6	135(3)	117.8
∠C-F1···H1	97.0	96.2	93(1)	98.4

[a] From Ref. [18].